High time resolution observation of $PM_{2.5}$ Brown carbon over Xi'an in northwestern China: Seasonal variation and source apportionment

Yali Lei, Zhenxing Shen, Tian Zhang, Di Lu, Yaling Zeng, Qian Zhang, Hongmei Xu, Naifang Bei, Xin Wang, Junji Cao

PII: S0045-6535(19)31754-0

DOI: https://doi.org/10.1016/j.chemosphere.2019.124530

Reference: CHEM 124530

To appear in: *ECSN*

Received Date: 10 June 2019

Revised Date: 2 August 2019

Accepted Date: 5 August 2019

Please cite this article as: Lei, Y., Shen, Z., Zhang, T., Lu, D., Zeng, Y., Zhang, Q., Xu, H., Bei, N., Wang, X., Cao, J., High time resolution observation of $PM_{2.5}$ Brown carbon over Xi'an in northwestern China: Seasonal variation and source apportionment, *Chemosphere* (2019), doi: https://doi.org/10.1016/j.chemosphere.2019.124530.

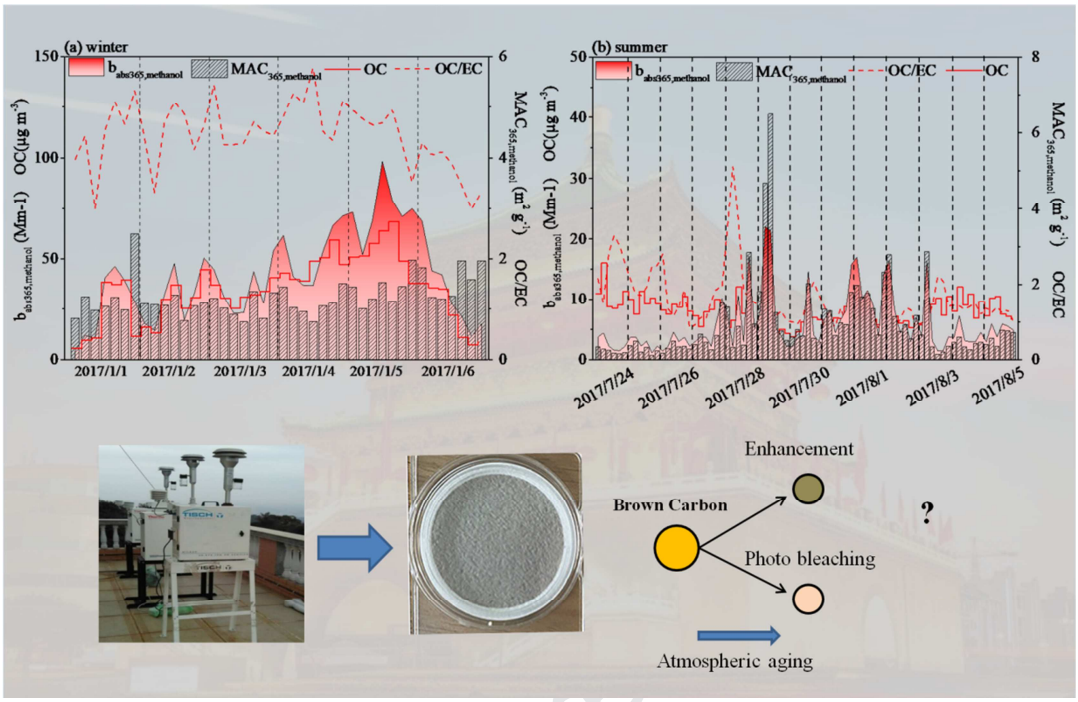

Daily variations of $b_{abs365,methanol}$, $MAC_{365,methanol}$, OC, OC/EC during winter and summer.

High Time Resolution Observation of $PM_{2.5}$ Brown Carbon over Xi'an in Northwestern China: Seasonal Variation and Source Apportionment

Yali Lei[1,2], Zhenxing Shen[1,2]*, Tian Zhang[1], Di Lu[1], Yaling Zeng[1], Qian Zhang[1], Hongmei Xu[1], Naifang Bei[3], Xin Wang[4], Junji Cao[2]

[1] *Department of Environmental Science and Engineering, Xi'an Jiaotong University, Xi'an 710049, China*

[2] *The State Key Laboratory of Loess and Quaternary Geology, Institute of Earth Environment, Chinese Academy of Sciences, Xi'an, 710049, China*

[3] *School of Human Settlements and Civil Engineering, Xi'an Jiaotong University, Xi'an, 710049, China*

[4]*Multiphase Chemistry Department, Max Planck Institute for Chemistry, Mainz, 55128, Germany*

**Author to whom correspondence should be addressed. E-mail: zxshen@mail.xjtu.edu.cn (Zhenxing Shen).*

Abstract

There is growing evidence suggesting the enhancement of brown carbon (BrC) in severe haze episodes. In this study, hourly measurements of BrC in $PM_{2.5}$ were conducted in Xi'an, a typical city in northwestern China during winter and summer. The absorption coefficient for methanol exacts at 365 nm ($b_{abs365,\ methanol}$, which is typically used as a proxy of methanol-soluble BrC) in the winter sampling period was over 7 times than that in summer. The mass absorption cross-section for methanol extracts ($MAC_{365,\ methanol}$, normalized by $b_{abs365,\ methanol}$ to organic carbon, OC) in winter sampling period was nearly 1.5 times of that in the summer. During the winter haze days, the average $b_{abs365,\ methanol}$ peaked at midnight and the lowest values in the morning, in contrast to high levels in afternoon and low levels at night in non haze days. Unlike the diurnal patterns in winter, summer $b_{abs365,\ methanol}$ diurnal variation presented high midday and low afternoon levels in haze days. However, in non haze days, the pattern showed high morning levels and night low levels. Haze and non haze variations of chemical species levels, $b_{abs365,\ methanol}$, and $MAC_{365,\ methanol}$ during winter and summer sampling time showed that the effects of atmospheric aging were complex and could either enhance or reduce light absorption of BrC. Source apportionment based on positive matrix factorization receptor model and multiple linear regressions showed that primary emission was an important contributor to BrC emissions during the winter sampling period, whereas secondary formation played an important role in summer.

Keywords: Brown carbon; High-time resolved; Source apportionment; Xi'an

1. Introduction

Brown carbon (BrC) is currently receiving remarkable attention because it is more abundant than black carbon (BC) and is a vital contributor to light absorption and climate forcing (*Lambe et al., 2013; Zhao et al., 2015*). Overall, emissions of primary BrC have been attributed to forest fires and biomass burning, residential heating, and biogenic release of humic matter (*Kirchstetter et al., 2004; Hoffer et al., 2006*). BrC can also be secondarily produced by photooxidation of anthropogenic and biogenic precursors (*Huang et al., 2017*). Such precursors like isoprene, toluene, and polycyclic aromatic naphthalene could yield BrC through heterogeneous or multiphase reactions (*Laskin et al., 2015; Liu et al., 2015*). Secondary BrC produced around urban environments can have an important influence on ultraviolet irradiance and photochemical cycles of urban pollution. For example, *Liu et al (2015)* illustrated that BrC influenced the production of O_3 and OH by reducing UV irradiance and consequently affected the oxidation capacity of the regional atmosphere. *Zhao et al (2015)* concluded that the magnitude of photo-enhancement and bleaching was likely dependent on the BrC components, as well as OH exposure.

Previous studies were launched to investigate BrC light absorption and climate forcing (*Shen et al., 2017a; 2017b; Lei et al., 2018b; Park et al., 2018*). However, previous long-term ambient BrC measurements were routinely carried out using 24-h integrated filter sampling techniques which exhibited relatively low time resolution and introduced more sample handling artifacts. High time-resolved organic carbon (OC) data were used to investigate the diurnal variation of carbonaceous aerosols and their contributions to air pollution in China, such as Beijing (*Lin et al., 2009*), Shanghai (*Xu et al., 2018*), Guangzhou (*Hu et al., 2012*), and Hong Kong (*Huang et al., 2014*). To our knowledge, some literatures estimated the BC and BrC light absorption using Aethalometer model (AE31), which may suffer from the interference from light absorption by BC and mineral dust (*Shen et al., 2017b; Qin et al., 2018; Wang et al., 2018*). However, few studies have utilized highly time-resolved semi-continuous measurements to study the diurnal variation of BrC light absorption in

bulk solution. Although the conversion from optical properties of solution back to aerosol is not necessarily straightforward, studying light-absorbing organics in bulk solution provides important insights on the sources and formation processes of SOA measurements of BrC. More highly time resolved measurements of BrC can yield insights into the temporal distributions in the light absorption, and offer the potential for better understanding of their emission sources. Thus, the information about variable and complicated BrC in fine particles is needed.

In this study, high time resolved $PM_{2.5}$ samples were collected to investigate the time-series of BrC light absorption to focus on the diel pattern. In addition, the formation and source apportionment of BrC was also conducted. The result of this study will improve our understanding of the dynamic variation of BrC and clarify their roles in both winter and summer.

2. Methodology

2.1 Sample collection

The sampling site was located in the southeastern part of downtown of Xi'an, which is subject to severe heavy air pollution produced by surrounding residential areas and major traffic roads. Sampling was conducted on the roof of a 15 m-high building from 1 January 2017 to 6 January 2017 and from 24 July 2017 to 5 August 2017 at Xi'an Jiaotong University (Fig.1). A total of 120 $PM_{2.5}$ samples (42 for winter and 78 for summer) with time resolution of 3 or 4 hours were collected on Whatman 47 quartz filters (Whatman Inc., Maidstone, UK) by using a PQ200 ambient air particulate sampler (BGI Inc., USA) at a flow rate of 16.7 $L \cdot min^{-1}$. $PM_{2.5}$ samples were equilibrated using controlled temperature (20-23 ^{o}C) and relative humidity (35-45 %) desiccators for 24 h before and after sampling and their mass loadings were determined gravimetrically using a Sartorius MC5 electronic microbalance (±1 μg sensitivity; Sartorius, Göttingen, Germany). Details of quality assurance and control procedures can be found in our previous studies (*Shen et al., 2017; Lei et al., 2018a; 2018b*). According to the ambient air quality standards (AAQS) of China (GB3095-2012:http://kjs.mep.gov.cn/hjbhbz/bzwb/dqhjbh/qhjzlbz/201203/t20120302

_224165.htm) and the measured data in this study, pollution day was defined as that the 24 h average concentrations both $PM_{2.5}$ were twice times higher than the national AAQS-Grade II value ($PM_{2.5}$, 75 $\mu g \cdot m^{-3}$).

Insert Figure 1

2.2 Chemical analysis

$PM_{2.5}$ OC and elemental carbon (EC) were determined with a DRI Model 2001 Thermal/Optical Carbon Analyzer (Atmoslytic Inc., Calabasas, CA, USA) following the IMPROVE TOR protocol (*Chow et al., 2004; Cao et al., 2005*). The IMPROVE_A (Interagency Monitoring of Protected Visual Environments) protocol produces four OC fractions (OC1, OC2, OC3, and OC4 at 140□, 180□, 480□, and 580□, respectively in a 100 % He atmosphere); a pyrolyzed carbon fraction (OP, determined when reflected or transmitted laser light attained its original intensity after O_2 was added to the analysis atmosphere); and three EC fractions (EC1, EC2, and EC3 in a 98 % He/2 % O_2 atmosphere at 580□, 740□, 840□, respectively). OC was defined as OC1+OC2+OC3+OC4+OP and EC as EC1+EC2+EC3-OP (*Chow et al., 2004*). One fourth of each filter was used for analysis of water-soluble inorganic ions (Na^+, NH_4^+, K^+, Mg^{2+}, Ca^{2+}, F^-, Cl^-, NO_3^- and SO_4^{2-}) using ion chromatography (IC, Dionex 500, Dionex Corp, USA). Anions were analyzed using an ASII-HC column (Dionex Company) and 20 mM potassium hydroxide as the eluent. Cations were determined using a CS12A column (Dionex Company) with 20 mM methane sulfonic acid as the eluent. One in each group of ten samples was selected for duplicate measurements and blank filter ion concentrations were subtracted for quality control purposes. A detailed description of the ion analysis carried out in this study can be found in *Shen et al (2018a).*

2.3 Optical properties of methanol extracts

The light absorption spectra of the methanol extracts were measured with a UV-Vis spectrophotometer (UV-6100s) with 10 cm optical paths in the individual solvent. A 0.526 cm^2 punch of filters were extracted in 50 mL methanol (HPLC Grade, Fisher

Chemical) by 30 min of sonication. All extracts were filtered 1-3 times with a 25 mm diameter 0.45 µm pore size microporous membrane (Puradisc 25 TF, PTFE membrane) to remove the insoluble components.

Absorption spectra of methanol-soluble organic carbon (MSOC) were used to assess the b_{abs} as described by *Srinivas and Sarin (2014)*. The b_{abs} was calculated according to:

$$b_{abs\lambda,methanol} = (A_{\lambda,methanol} - A_{700,methanol}) * (V_{ext} * Portions) * ln(10) / (V_{aero} * L) \quad (1)$$

where b_{abs} is expressed in the unit of Mm^{-1} (or 10^{-6} m^{-1}). A_{λ} and A_{700} correspond to measured absorbance at specified λ and 700 nm, respectively. V_{ext} refers to volume of the solvent extract (50 mL) in which different portions of filter. *Portions* is used to estimate the absorption signal for the full filter. For example, if *Portions* is 8 which means 1/8th portions of aerosol filter are extracted. V_{aero} corresponds to sampling volume. In this case, *L* is the path length of the cell (10 cm). We used light absorbance at 365 nm to estimate BrC b_{abs} (*Liu et al., 2013*).

The relationship between wavelength-dependent *AAE* and b_{abs} of BrC in the methanol extracts is described as follows *(Hecobian et al., 2010)*:

$$b_{abs\lambda,methanol} = K * \lambda^{-AAE\ methanol} \quad (2)$$

Here *K* refers to a constant value and λ denotes the wavelength of BrC. In this study, *AAE* was calculated by linear regression fit to log b_{abs} vs. log λ in the wavelength range of 330-400 nm.

The soluble organic mass, unfortunately, cannot be determined in the methanol extracts. Therefore, OC measured from OC/EC analysis was used to obtain the lower limit of the MAC value at 365 nm, shown in equation (3):

$$MAC_{\lambda,methanol} = b_{abs\ \lambda\ methanol} / OC \quad (3)$$

2.4 BC absorption measurements

The particular b_{abs} of BC can be obtained from seven wavelengths (i.e., 370, 470, 520, 590, 660, 880, and 950 nm) using AE31. According to Beer-Lambert's law, the b_{abs} is defined as:

$$I = I_0 e^{-b_{abs} \cdot x} \quad (4)$$

where I_0 and I are the light intensities before and after collecting particles with the thickness x, respectively. Similar to other filter-based absorption instruments, the b_{abs} of AE31 needs to be corrected for two kinds of errors, including scattering effect by the fiber filter substrates (*Collaud Coen et al., 2010*) and filter mass loading by the accumulation of light absorbing particles (*Zhang et al., 2015b; Qin et al., 2018*). In this study, mass loading effect was corrected by following the correction process presented by *Virkkula et al (2007).* A detailed description of AE31 analysis followed in this study can be found in Shen et al., 2017b). *Olson et al (2015)* segregated BC and optical-BrC by projecting the absorption at higher wavelengths (880 nm) to lower wavelengths of the spectrum measured by the AE31. The absorption at 880 nm is assumed to be attributed to only BC absorption.

2.5 Source apportionment of $b_{abs365,\ methanol}$

In order to investigate the contributions of each emission source to $b_{abs365,\ methanol}$, positive matrix factorization (PMF) has been first used. PMF is a bilinear factor model that has been widely used in previous source apportionment studies (*Tao et al., 2014; Xiao et al., 2014; Wang et al., 2016*). The concept of PMF has been described in detail by *Shen et al. (2010).* In this study, water-soluble inorganic ions (NH_4^+, K^+, Mg^{2+}, Ca^{2+}, NO_3^-, and SO_4^{2-}), and carbon fractions (OC1, OC2, OC3, OC4, EC1, EC2, EC3) were used as data inputs. The model decomposes the concentrations of the chemical species related above at a receptor site into sets of contributions *(G)*, factor profiles *(F)*, and residuals *(E)*:

$$X_{ij} = \sum_{k=1}^{p} G_{ik} F_{kj} + E_{ij} \quad (5)$$

Where X_{ij} represents the *j*th species concentration measured in the *i*th sample, the factor time series G_{ik} is the contribution of the *k* source to the *i*th sample, the factor profile F_{kj} is the concentration of the *j*th species in the *k* source, and the model residuals are E_{ij}. The model uses a least-squares approach to iteratively minimize the object function *Q*, which is defined as the sum of the squared residuals weighted by uncertainties σ_{ij}:

$$Q = \sum_{i=1}^{m} \sum_{j=1}^{n} \left(\frac{E_{ij}}{\sigma_{ij}}\right)^2 \quad (6)$$

The model requires both concentration data X_{ij} and a corresponding uncertainty σ_{ij}. The σ_{ij} was calculated using the equation as follows:

$$Uncertainty = \sqrt{([\mathrm{X}] \times CV)^2 + MDL^2} \quad \text{, for [X]>MDL} \quad (7)$$

$$Uncertainty = \frac{5}{6} \times MDL \quad \text{, for [X]}\leq\text{MDL} \quad (8)$$

Where [X] represents the concentration of the species X in $\mu g \cdot m^{-3}$; CV is the coefficient of variation for species X, which is calculated by dividing the standard deviation of repeated samples by their average value; MDL is the method detection limit.

The PMF model was run multiple times, extracting four to six factors, and each run was initialized with different starting points (changing the seed value from 1 to 20).

A multivariate linear regression model was constructed, which has been described in detail by *Lei et al. (2018b)*.

The relationships between $b_{abs365,methanol}$ and each emission source can be described as:

$$b_{abs365,methanol} = B + \sum_{i,j=1}^{n} A_i \times [\mathrm{X_{ij}}] \quad , \quad (9)$$

Where the quantities in brackets $[X_{ij}]$ represent the contributions of the i-th emission source (units: Mm^{-1}) on the j-th day; A_i and B represent the regression coefficient and random error respectively; $A_i \times [X_{ij}]$ represents the predicted values of $b_{abs365,methanol}$ from the i-th emission source.

3. Results and Discussion

3.1 Overview of winter and summer intensive observation

Winter and summer mean values of $PM_{2.5}$ chemical species, $b_{abs365,\ methanol}$, $AAE_{methanol}$ (330-400 nm), and $MAC_{365,\ methanol}$ during the sampling period were

summarized in Table 1. The daily mean concentrations of $PM_{2.5}$ in winter sampling period varied from 109.5 to 286.6 μg m^{-3} with an average of 179.4 ±70.4 μg m^{-3}, which was twice higher than that in summer sampling period. These measured values matched the previous reported seasonal variation of OC and EC concentration at Xi'an (*Shen et al., 2017b*), with lower value in summer and high in winter. The high average concentration of secondary organic carbon (SOC) and OC/EC demonstrated the higher secondary emissions. Winter average $b_{abs365,\ methanol}$ is over 7 times than that in summer sampling period, indicating more abundance of BrC in winter $PM_{2.5}$ samples in comparison with summer. Biomass burning in rural areas around Xi'an for winter heating should contribute to high BrC, the evidence of which can be found in previous studies (*Sun et al., 2017; Shen et al., 2017a; Lei et al., 2018a*). The *AAE* (330-400 nm) values were 6.2±0.5 during winter sampling period and 6.5±2.6 during summer sampling period. In a previous study, it was found that high SOC levels were occurred both in summer and winter $PM_{2.5}$ over Xi'an, even their seasonal formation mechanisms were difference (*Zhang et al., 2015a*). Winter $MAC_{365,methanol}$ for BrC was nearly 1.5 times higher than that in summer during this sampling period, highlighting that BrC from biomass burning and fresh SOC caused stronger light absorption than that from the aged SOC in summer. The average b_{abs} of BC at 880 nm ($b_{abs\text{-}BC,\ 880\ nm}$) was 101.9 Mm^{-1} for winter sampling period and 11.8 Mm^{-1} for summer sampling period, also indicating the important contribution from primary emission sources in winter. It is noted that the mean $b_{abs\text{-}BC,\ 880\ nm}$ was more than twice as high as $b_{abs365,\ methanol}$ for both in winter and summer during our sampling period, highlighting that PM light absorption was predominantly by BC in Xi'an.

Insert Table 1

3.2 Winter brown carbon profiles

Fig.2a displays the average diurnal trends of $b_{abs365,\ methanol}$, $b_{abs,\ BC\text{-}880\ nm}$, $MAC_{365,\ methanol}$, OC, as well as SOC between haze and non haze days during the winter sampling period. $b_{abs365,\ methanol}$ diurnal variation presented high midnight time levels

and low morning levels in haze days, which is similar to results in another study in Guangzhou, China (*Qin et al., 2018*). This pattern results from the variation of the boundary layer and inversion layers. At night, the level of the boundary layer goes down with decreased solar activity, and the inversion layer occur (*Wang et al., 2007; Xu et al., 2014; Shen et al., 2011*). As shown in Figure S1, in haze days, $b_{abs365,\ methanol}$ diurnal variation presented higher midnight time levels, which is mainly due to the reason that the level of the boundary layer goes down with decreased solar activity and the inversion layer occurs. Moreover, nighttime aqueous-phase chemistry also affects this phenomenon (*Folkers, et al., 2003; Rajput et al., 2016; Saffai, et al., 2016*). However, in non haze days, the pattern showed higher in afternoon levels and low in night time levels. $MAC_{365,methanol}$ exhibited no obvious changes and showed relatively high night time levels in both haze and non haze days. OC showed no distinctive early morning peaks in both haze days and non haze days. The enhanced OC concentrations at around midday likely reflected the contribution of SOC formed via photochemical activities. SOC diel variations showed higher at noon and lower in the nighttime. A previous study in the Pearl River Delta region suggested that strong photochemical formation was responsible for the midday SOC peak (*Xu et al., 2017*). Similar midday SOC peaks have also been identified in several other urban areas, such as the Los Angeles Basin during the CalNex-2010 field campaign (*Zhang et al., 2013*) and Mexico City during the MILAGRO study (*Gouw et al., 2009*). As a result, the increase of OC and SOC suggests that photochemical processes were a primary driver in the formation of BrC. In addition, the oxidant (Ox) discussed here is the sum of the ozone and nitrogen dioxide mixing ratios (O_3+NO_2), which can be considered as a proxy for atmospheric oxidation level caused by photochemical reactions (*Wang et al., 2017*). The mixing ratio of Ox was used to represent the atmospheric oxidation capacity. Significant variations in the time-resolved of Ox were observed over Xi'an, with mixing ratios ranging from 32.0 to 84.8 ppb and averaging 14.5 ± 55.4 ppb during the winter sampling period, respectively. The daily Ox minimum occurred at morning time followed by a sharp increase to a nighttime peak at midnight in haze days. However, for non haze days, the Ox peaked at 14:00 and then declined

continuously until the midnight. It is likely driven by variations in local anthropogenic activities, photochemical conditions, and atmospheric boundary layer heights.

Insert Figure 2

Diurnal patterns of $b_{abs\text{-}BC,\ 880\ nm}$ in haze and non haze days during winter sampling period were also exhibited in Fig 2b. In haze days, BC light absorption showed no specific peaks. Despite the rush hours, some VOCs may uptake to BC particles and enhance the light absorption (*Qin et al., 2018*). Similar results have also been found in other studies (*Xu, et al., 2014; Wang et al., 2016b; 2016c*). However, in non haze days, BC light absorption showed only one peak at around 10:00-14:00 LST. On one hand, the vehicular emissions rates during the morning rush hours were generally higher than those in the evening rush hours as the morning traffic congestion was severer than that in the evening rush hours as reported by a road tunnel study (*Zhou et al., 2014*) in the same borough. The lowest BC light absorption at midday should be mainly ascribed to development of boundary layer as the solar radiation was the strongest at that time.

In this study, differences of $PM_{2.5}$ chemical species and BrC optical properties between haze and non haze can provide some insights of on BrC formation and optical properties. As shown in Table 1, winter OC/EC ratios showed little higher than non haze, indicating that the SOC formation intensity were similar between haze and non haze days. In contrast, winter haze OC and SOC levels as well as $b_{abs365,\ methanol}$ were much higher than those in non haze days, implied that primary emissions and secondary formation played an important contribution to winter haze BrC.

3.3 Profiles of brown carbon in summer

The average diurnal trends of $b_{abs365,\ methanol}$, $b_{abs,\ BC\text{-}880\ nm}$, $MAC_{365,\ methanol}$, OC, Ox, as well as SOC between haze and non haze days during summer sampling period were shown in Fig. 2b. Unlike the diurnal patterns during winter, summer $b_{abs365,\ methanol}$ diurnal variation presented high midday and low afternoon levels in haze days.

However, in non haze days, the pattern showed higher morning levels and lower night time levels. OC presented distinct diurnal patterns during the daytime. $MAC_{365,\ methanol}$ showed relatively higher in the morning during haze days and at midday during non haze days. The enhanced OC concentrations at around midday in non haze days likely reflected the contribution of SOC formed via photochemical activities. The Ox minimum occurred at morning time followed by a sharp increase to peak at around 20:00 LST in haze days. However, for non haze days, the Ox peaked at 8:00 LST and then declined continuously until the midnight. Ox mixing ratios shows that $b_{abs365,methanol}$ exhibited similar diurnal patterns during winter and summer (*Tang et al 2012, Feng et al 2016).*

It is likely driven by variations in local anthropogenic activities, photochemical conditions, and atmospheric boundary layer heights. Ox mixing ratios shows that $b_{abs365,methanol}$ exhibited similar diurnal patterns during our winter and summer sampling period. Diurnal patterns of $b_{abs\text{-}BC,\ 880\ nm}$ in haze and non haze days during the summer sampling period were also displayed in Fig.2b. BC light absorption showed two evident peaks at around 7:00-9:00 LST and 20:00-2:00 LST (the next day) in both haze and non haze days, tracking with the morning rush hours due to the enhanced vehicular emission rates during the traffic rush hours and shallow mixing layer heights. In both haze and non haze days, the morning peaks of BC were consistently higher than the evening peaks.

Summer levels of $PM_{2.5}$ chemical species showed no evident difference between haze and non haze, but they were twice lower than that in winter, which mainly because of extra biomass burning for winter heating (*Lei et al., 2018a*). EC, which was mainly from primary emission sources, was in the same level between haze and non haze periods. It was noted that haze SOC and $b_{abs365,\ methanol}$ were a little higher than non haze, which indicated that SOC-BrC was abundance in haze than in non haze period. In addition, haze $MAC_{365,\ methanol}$ was about 1.4 time than non haze, which inferred that relatively photochemical reactions can lead to high light absorption as a result of formation of chromophores by atmospheric aging. However, the effects of atmospheric aging are complex and can either enhance or reduce light absorption by

BrC. Variations of molecular composition and their optical properties of BrC should be conducted among the different SOC formations in the future.

3.4 Source apportionment of brown carbon

In this study, a PMF model was first conduced to apportion $PM_{2.5}$ sources， then a multivariate linear regression model was used to investigate the contribution of each source to $b_{abs365,\ methanol}$ in both winter and summer sampling period. Table S1 shows regression diagnosis for each individual species and total $PM_{2.5}$ mass obtained by the PMF model.

Figure S2 shows source profiles of each source to $PM_{2.5}$ in winter. Factor 1 was characterized by Ca^{2+}, NO_3^-, EC1, and EC2, which were characteristic of traffic-related emissions (*Shakeri et al., 2016*). Factor 2 loaded with sulfate, OC and EC, representing emissions from coal combustion (*Huang et al., 2013; Shakeri et al., 2016*). Biomass burning emissions were identified as Factor 3 was abundance of K^+ (*Shen et al., 2010; Shakeri et al., 2016*). Factor 4 loaded with NH_4^+, NO_3^-, and SO_4^{2-}, indicating a secondary formation source (*Shen et al., 2010*). The contributions of the sources resulting from the PMF analyses were calculated by multiple regression of the G matrix (*Paatero, 1994*) against the measured mass concentrations. Secondary formation source contributed significantly to the detected $PM_{2.5}$ mass (37.7 %), followed by traffic-related emissions (24.8 %), biomass burning (19.4 %), coal combustion (18.1 %) (Figure S3).

Insert Figure S1

Insert Figure S2

However, during summer traffic-related emissions contributed significantly to the $PM_{2.5}$ mass (36.1 %), followed by fugitive dust (27.3 %), sulfate and SOA (17.5 %), nitrate and SOA (12.0 %) and industrial coal combustion (7.2 %) (Figure S5). The source profiles of five sources to $PM_{2.5}$ in summer were showed in Figure S4. Factor 1 was dominated by SO_4^{2-} and NH_4^+, which were characteristic of sulfate and its

secondary formation (*Li et al., 2013*). Factor 2 loaded with Mg^{2+} Ca^{2+} and K^{+}, representing emissions from fugitive dust (*Shen et al., 2008; Zhang et al., 2014*). Factor 3 was characterized by Ca^{2+}, NO_3^-, EC1, and EC2, which was thought to be associated with traffic-related emissions (*Shakeri et al., 2016*). Factor 4 had high loadings on SO_4^{2-}, OC and EC, which gave preliminary indications of emissions from industrial coal combustion. Nitrate and its secondary formation were identified as Factor 5 was abundance of NH_4^+ and NO_3^- (*Shen et al., 2010; Zhou et al., 2017*).

Insert Figure S3

Insert Figure S4

Figure 3 shows the source contributions to $b_{abs365,\ methanol}$ obtained using a multivariate linear regression model during winter (a) and summer (b). Because dust was not present in the solvent extract, fugitive dust could not be investigated in the apportioning of $b_{abs365,\ methanol}$. Therefore, almost 71.6 % (winter) and 82.7 % (summer) of $b_{abs365,\ methanol}$ were apportioned in this study. The primary emissions during winter including biomass burning, coal combustion, and traffic emissions were 23.1 ± 20.8 Mm^{-1}, 14.7 ± 12.2 Mm^{-1} and 10.4 ± 6.8 Mm^{-1}, respectively. The primary emissions related above accounted for more than 40 % of the total $b_{abs365,\ methanol}$ The averaged $b_{abs365,\ methanol}$ of secondary formation during winter was 25.6 ± 12.1 Mm^{-1}, accounting for 28.0 % of total $b_{abs365,\ methanol}$. While for summer, about 74.5 % of the total $b_{abs365,\ methanol}$ was associated with secondary formation including sulfate (42.4 %) and nitrate (32.1 %), which was almost three times higher than that for winter. It was inferred that primary emission was an important contributor to BrC emissions during winter while secondary formation played an important role during summer.

Insert Figure 3

4. Conclusions

In this study, highly time-resolved BrC in $PM_{2.5}$ was conducted in Xi'an, a typical city in northwestern China. We discussed the seasonal, diurnal profiles of BrC during haze and non haze days.

Winter average $b_{abs365,methanol}$ is over 7 times than that in summer during the sampling period. Winter $MAC_{365,methanol}$ for BrC was nearly 1.5 times of that in summer. During winter sampling period, $b_{abs365,\ methanol}$ diurnal variation presented high night time levels and low morning levels in haze days while in non haze days, the pattern showed higher in afternoon levels and low in night time levels. Unlike the diurnal patterns in winter sampling period, $b_{abs365,\ methanol}$ diurnal variation presented high midday and low afternoon levels in haze days. However, in non haze days, the pattern showed higher in morning levels and low in night time levels. Winter SOC-BrC may exist due to photobleaching reaction, while summer photochemical reactions may form chromophores which led to high light absorption. Source apportionment based on PMF showed that during winter, secondary formation source contributed significantly to $PM_{2.5}$ mass, followed by traffic-related emissions (24.8 %), biomass burning (19.4 %), and coal combustion (18.1 %) while during summer traffic-related emissions contributed significantly to $PM_{2.5}$, followed by fugitive dust (27.3 %), sulfate and its secondary formation (17.5 %), nitrate and its secondary formation (12.0 %) and industrial coal combustion (7.2 %). The results from the multiple linear regression $b_{abs365,\ methanol}$ source contribution highlighted that primary emission and secondary formation were important contributors to BrC emissions in winter and summer, respectively. Molecular composition and optical properties in summer and winter should be conducted in the future.

Acknowledgements

This research is financially supported by the Natural Science Foundation of China (grants 41877383, 41573101), Natural Science Basic Research Plan in Shaanxi Province of China (Grant No 2016JQ4019), and a grant from SKLLQG, Chinese Academy of Sciences (SKLLQG1616).

References

Cao, J.J., Wu, F., Chow, J.C., Lee, S.C., 2005. Characterization and Source Apportionment of Atmospheric Organic and Elemental Carbon during Fall and Winter of 2003 in Xi'an, China. Atmos. Chem. Phys. 5(11), 3127-3137.

Chow, J.C., Watson, J.G., Chen, L.W.A., Arnott, W.P., Moosmüller, H., 2004. Equivalence of elemental carbon by thermal/optical reflectance and transmittance with different temperature protocols. Environ. Sci. Technol. 38, 4414-4422.

Collaud Coen, M., Weingartner, E., Apituley, A., Ceburnis, D., Fierz-Schmidhauser, R., Flentje, H., Henzing, J., Jennings, S.G., Moerman, M. and Petzold, A. (2010). Minimizing Light Absorption Measurement Artifacts of the Aethalometer: Evaluation of Five Correction Algorithms. Atmos. Meas. Tech. 3: 457-474.

Dalirian, M., Ylisirniö, A., Buchholz, A., Schlesinger, D., Ström, J., Virtanen, A. and Riipinen, I. (2017). Cloud Droplet Activation of Black Carbon Particles Coated with Organic Compounds of Varying Solubility. Atmos. Chem. Phys. Discuss. https://doi.org/10.5194/acp-2017-1084.

Feng, T., Bei, N.F., Huang, R.J., Cao, J.J., Zhang, Q., Zhou, W.J., Tie, X.X., Liu, S.S., Zhang, T., Su, X.L., Lei, W.F., Molina, L.T., Li, G.H., 2016. Summertime ozone formation in Xi'an and surrounding areas, China. Atmos. Chem. Phys. 16, 4323-42.

Folkers, M., Mentel,, F., Wahner, A., 2003. Influence of an organic coating on the reactivity of aqueous aerosols probed by the heterogeneous hydrolysis of N2O5. Geophys, Res. Lett. doi:10.1029/2003GL017168.

Gouw, J.D., Welsh-Bon, D., Warneke, C., Kuster, W., Alexander, L., Baker, A.K., Beyersdorf, A.J., Blake, D., Canagaratna, M., Celada, A., 2009. Emission and chemistry of organic carbon in the gas and aerosol phase at a sub-urban site near Mexico City in March 2006 during the MILAGRO study. Atmos. Chem. Phys. 9, 3425-3442.

Hecobian, A., Zhang, X., Zheng, M., Frank, N., Edgerton, E.S., Weber, R.J., 2010. Water-Soluble Organic Aerosol material and the light-absorption characteristics of aqueous extracts measured over the Southeastern United States. Atmos. Chem. Phys. 10, 5965-5977.

461 Hoffer, A., Gelencser, a., Guyon, P., Kiss, G.G., 2006. Optical properties of humic-like substances
462 (HULIS) in biomass-burning aerosols. Atmos. Chem. Phys. 5(4), 3563-3570.
463 Hu,W., Hu, M., Deng, Z., Xiao, R., Kondo, Y., Takegawa, N., Zhao, Y., Guo, S., Zhang, Y., 2012.
464 The characteristics and origins of carbonaceous aerosol at a rural site of PRD in summer of
465 2006. Atmos. Chem. Phys. 12, 1811-1822.
466 Huang, X.H.H., Bian, Q.J., Louie, P.K.K., Yu, J.Z., 2014. Contributions of vehicular carbonaceous
467 aerosols to PM2.5 in a roadside environment in Hong Kong. Atmos. Chem. Phys. 14, 9279-
468 9293.
469 Huang, M.Q., Xu, J., Cai, S.Y., Liu, X.Q., Zhao, W.X., Hu, C.J., Gu, X.J., Fang, Li, Zhang, W.J.,
470 2017. Characterization of brown carbon constituents of benzene secondary organic aerosol aged
471 with ammonia. J. Atmos. Chem. D05203, 1-14.
472 Kirchstetter, T.W., Novakor, T., Hobbs, P.V., 2004. Evidence that the spectral dependence of light
473 absorption by aerosols is affected by organic carbon. J. Geophys. Res. 109, D21208,
474 doi:10.1029/2004JD004999.
475 Lambe, A.T., Cappa, C.D., Massoli, P., Onasch, T.B., Forestieri, S.D., Martin, A.T., Cummings,
476 M.J., Croadale, D.R., Brune,W.H.,Worsnop, D.R., Davidovits, P., 2013. Relationship between
477 oxidation level and optical properties of secondary organic aerosol. *Environ. Sci. Technol.* 47
478 (12), 6349-6357.
479 Laskin, A., Laskin, J., Nizkorodov, S.A., 2015. Chemistry of Atmospheric brown carbon. Chem.
480 Rev. 115(10).
481 Lei, Y.L., Shen, Z.X., Zhang, T., Zhang, Q., Wang, Q.Y., Sun, J., Gong, X.S., Cao, J.J., Xu, H.M.,
482 Liu, S.X., Yang, L., 2018a. Optical source profiles of brown carbon in size-resolved particulate
483 matter from typical domestic biofuel burning over Guanzhong Plain, China. Sci. Total. Environ.
484 622-623, 244-251.
485 Lei, Y.L., Shen, Z.X., Wang, Q.Y., Zhang, T., Cao, J.J., Sun, J.J., Zhang, Q., Wang, L.Q., Xu,
486 H.M., Tian, J., Wu, J.M., 2018b. Optical characteristics and source apportionment of brown
487 carbon in winter PM2.5 over Yulin in Northern China. Atmos. Res. 213, 27-33.
488 Li, J.J., Wang, G.H., Cao J.J., Wang, X.M., Zhang, R.J., 2013. Observation of biogenic secondary
489 organic aerosols in the atmosphere of a mountain site in central China: temperature and relative
490 humidity effects, Atmos. Chem. Phys., 13(22), 11535-11549.

Li-Jones, X., Prospero, J.M., 1998. Variations in the size distribution of non-sea-salt sulfate aerosol in the marine boundary layer at Barbados: impact of African dust. J. Geophys. Res. 103, 16073-16084.

Lin, P., Hu, M., Deng, Z., Slanina, J., Han, S., Kondo, Y., Takegawa, N., Miyazaki, Y., Zhao, Y., Sugimoto, N., 2009. Seasonal and diurnal variations of organic carbon in PM2.5 in Beijing and the estimation of secondary organic carbon. J. Geophys. Res. Atmos. 114, D00G11.

Liu, J., Bergin, M., Guo, H., King, L., Kotra, N., Edgerton, E., Weber, R.J., 2013. Size resolved measurements of brown carbon in water and methanol extracts and estimates of their contribution to ambient fine-particle light absorption. Atmos. Chem. Phys. 13 (24), 12389-12404.

Liu, P.F., Abdelmalki, N., Hung, H.-M., Wang, Y., Brune,W.H., Martin, S.T., 2015. Ultraviolet and visible complex refractive indices of secondary organic material produced by photooxidation of the aromatic compounds toluene and m-xylene. Atmos. Chem. Phys. 14(14), 20585-20615.

Olson, M.R., Victoria Garcia, M., Robinson, M.A., Van Rooy, P., Dietenberger, M.A., Bergin, M. and Schauer, J.J. (2015). Investigation of Black and Brown Carbon Multiple - Wavelength - Dependent Light Absorption from Biomass and Fossil Fuel Combustion Source Emissions. J. Geophys. Res. Atmospheres 120, 6682-6697.

Paatero, P., and Tapper, U., 1994. Positive matrix factorization: A non-negative factor model with optimal utilization of error estimates of data values. Environmetrics. 5(2), 111-126.

Park, S.S., Yu, G.H., Lee, S., 2018. Optical absorption characteristics of brown carbon aerosols during the KORUS-AQ campaign at an urban site. Atmos. Res. 203, 16-27.

Qin, Y.M., Tan, H.B., Li, Y.J., Li, Z.J., Schurman, M.I., Liu, L., Wu, C., Chan, C.K., 2018. Chemical characteristics of brown carbon in atmospheric particles at a suburban site near Guangzhou, China. Atmos. Chem. Phys. 18, 16409-16418.

Rajput, P., Gupta, T., Kumar, A., 2016. The diurnal variability of sulfate and nitrate aerosols during winter time in the Indo-Gangetic Plain: implications for heterogeneous phase chemistry. RSC Adv.6, 89879-89887.

Saffari, A., Hasheminassab, S., Shafer, M., Schauer, J.J., Chatila, T.A., Sioutas, C., 2016. Nighttime aqueous-phase secondary organic aerosols in Los Angeles and its implication for fine particulate matter composition and oxidative potential. Atmos. Environ. 133, 112-122.

Saleh, R., Hennigan, C.J., McMeeking, G.R., Chuang, W.K., Robinson, E.S., Coe, H., Donahue, N.M., Robinson, A.L., 2013. Absorptivity of brown carbon in fresh and photo-chemically aged biomass-burning emissions. Atmos. Chem. Phys. 13, 7683-7693.

Seinfeld, J.H., 1986. Atmospheric Chemistry and Physics of Air Pollution. Wiley, New York.

Shen, Z.X., Arimoto, R., Cao, J.J., Zhang, R.J., Li, X.X., Du, N., Okuda, T., Nakao, S., Tanaka, S., 2008. Seasonal variations and evidence for the effectiveness of pollution controls on water-soluble inorganic species in total suspended particulates and fine particulate matter from Xi'an, China. J. Air Waste Manag. Assoc. 58, 1560-1570.

Shen, Z.X., Cao, J.J., Arimoto, R., Han, Y.M., Zhu, C.S., Tian, J., Liu, S.X., 2010. Chemical characteristics of fine particle (PM1) from Xi'an, Chia. Aerosol Sci. & Technol. 44(6), 461-472.

Shen, Z.X., Zhang, Q., Cao, J.J., Zhang, L.M., Lei, Y.L., Huang, Y., Huang, R.J., Gao, J.J., Zhao, Z.Z., Zhu, C.S., Yin, X.L., Zheng, C.L., Xu, H,M., Liu, S.X., 2017a. Optical properties and possible sources of brown carbon in $PM_{2.5}$ over Xi'an, China. Atmos. Environ. 150, 322-330.

Shen, Z.X., Lei, Y.L., Zhang, L.M., Zhang, Q., Zeng, Y.L., Tao, J., Zhu, C.S., Cao, J.J., Xu, H.M., Liu, S.X., 2017b. Methanol extracted Brown Carbon in $PM_{2.5}$ over Xi'an, China: Seasonal variation of optical properties and sources identification. Aerosol. Sci. Engineering 1-9.

Shakeri, A., Madadi, M., Mehrabi, B., 2016. Health risk assessment and source apportionment of PAHs in industrial and bitumen contaminated soils of Kermanshah province; NW Iran. Toxicol. & Environ. Health. Sci. 8(3), 201-212.

Srinivas, B., Sarin, M.M., 2014. Brown carbon in atmospheric outflow from the Indo-Gangetic Plain: Mass absorption efficiency and temporal variability. J. Atmos. Environ. 89, 835-843.

Tang, G., Wang, Y., Li, X., Ji, D., Hsu, S. and Gao, X., 2012. Spatial temporal variations in surface ozone in Northern China as observed during 2009–2010 and possible implications for future air quality control strategies Atmos. Chem. Phys. 12, 2757-76.

Tao, J., Zhang, L.M., Cao, J.J., Zhang, R.J., 2017. A review of current knowledge concerning PM2.5 chemical composition, aerosol optical properties, and their relationships across China. Atmos. Chem. Phys. 1-70.

Virkkula, A., Makela, T., Hillamo, R., Yli-Tuomi, T., Hirsikko, A., Hameri, K., Koponen, I.K., 2007. A simple procedure for correcting loading effects of aethalometer data. J. Air Waste Manage. 57(10), 1214-1222.

Wang, G.H., Kawamura, K., Zhao, X., Li, Q.G., Dai, Z.X., Niu, H.Y., 2007. Identification, abundance seasonal variation of anthropogenic organic aerosols from a mega-city in China. Atmos. Environ. 41, 407-416.

Wang, J., Nie, W., Cheng, Y., Shen, Y., Chi, X., Wang, J., Huang, X., Xie, Y., Sun, P., Xu, Z., Qi, X., Su, H. and Ding, A., 2018. Light absorption of brown carbon in eastern China based on 3-year multi-wavelength aerosol optical property observations and an improved absorption Ångström exponent segregation method, Atmos. Chem. Phys. 18(12), 9061-9074.

Wang, Q.Y., Huang, R.J., Zhao, Z.Z., Cao, J.J., Ni, H.Y., Tie, X.X., Zhao, S.Y., Su, X.L., Han, Y.M., Shen, Z.X., Wang, Y.C., Zhang, N.N., Zhou, Y.Q., Corbin, J.C., 2016a. Physicochemical characteristics of black carbon aerosol and its radiative impact in a polluted urban area of China. J. Geophys. Res. Atmos. 121(20), 12505-12519.

Wang, J.F., Ge, X.L., Chen, Y.F., Shen, Y.F., Zhang, Q., Sun, Y.L., Xu, J.Z., Ge, S., Yu, H., Chen, M.D., 2016b. Highly time-resolved urban aerosol characteristics during springtime in Yangtze River Delta, China: insights from soot particle aerosol mass spectrometry. Atmos. Chem. Phys. 16, 9109-9127.

Wang, J.F., Onasch, T.B., Ge, X.L., Collier, S., Zhang, Q., Sun, Y.L., Yu, H., Chen, M.D., Prevot, A.S.H., Worsnop, D.R., 2016c. Observation of fullerene soot in eastern China. Environ. Sci. Technol, Lett. 3, 121-126.

Wang, Q.Y., Huang, R.J., Zhao, Z.Z., Cao, J.J., Ni, H.Y., Tie, X.X., Zhu, C.S., Shen, Z.X., Wang, M., Dai, W.T., Han, Y.M., Zhang N.N., Prevot, A.S.H., 2017. Effects of photochemical oxidation on the mixing state and light absorption of black carbon in the urban atmosphere of China. Environ. Res. Lett. 12, 044012.

Xiao, S., Wang, Q.Y., Cao, J.J., Huang, R.J., Chen, W.D., Han, Y.M., Xu, H.M., Liu, S.X., Zhou, Y.Q., Wang, P., Zhang, J.Q., Zhan, C.L., 2014. Long-term trends in visibilty and impacts of aerosol composition on visibility impairment in Baoji, China. Atmos. Res. 149, 88-95.

Xu, J., Zhang, Q., Chen, M., Ge, X., Ren, J., Qin, D., 2014. Chemical composition, sources, processes of urban aerosols during summertime in northwest China, insights from high resolution aerosol mass spectrometry. Atmos. Chem. Phys. 14, 12593–12611.

Xu, J., Wang, Q.Z., Deng, C.R., McNeill, V.F., Fankhauser, A., Wang, F.W., Zheng, X.J., Shen, J.D., Huang, K., Zhuang, G.S., 2018. Insights into the characterisitic and sources of primary and

secondary organic carbon: High time resolution observation in urban Shanghai. Environ. Pollut. 233, 1177-1187.

Yan, C.Q., Zheng, M., Sullivan, A.P., Bosch, C., Desyaterik, Y., Andersson, A., Li, X.Y., Guo, X.S., Zhou, T., Gustafsson, O., Collett Jr, J.L., 2015. Chemical characteristics and light-absorbing property of water-soluble organic carbon in Beijing: Biomass burning contributions. Atmos. Environ. 121, 4-12.

Zhang, Q., Shen, Z.X., Cao, J.J., Ho, K.F., Zhang, R.J., Bie, Z.J., Chang, H.R., Liu, S.X., 2014. Chemical profiles of urban fugitive dust over Xi'an in the south margin of the Loess Plateau, China. Atmos. Pollut. Res. 5(3), 421-430.

Zhang, Q., Shen, Z.X., Cao, J.J., Zhang R.J., Zhang, L.M., Huang, R.J., Zheng, C.J., Wang, L.Q., Liu, S.X., Xu, H.M., Zheng, C.L., Liu, P.P., 2015a. Variations in $PM_{2.5}$, TSP, BC, and trace gases NO_2, SO_2 and O_3 between haze and non-haze episodes in winter over Xi'an, China. Atmos. Environ. 112, 64-71.

Zhang, X.L., Lin, Y.H., Surratt, J.D., Weber, R.J., 2013. Sources, composition and absorption Ångström exponent of light-absorbing organic components in aerosol extracts from the Los Angeles Basin. Environ. Sci. Technol. 47, 3685-3693.

Zhang, X.L., Mao, M., 2015b. Brown haze types due to aerosol pollution at Hefei in the summer and fall. Chemosphere. 119, 1153-1162.

Zhao, R., Lee, A.K.Y., Huang, L., Li, X., Yang, F., Abbatt, J.P.D., 2015. Photochemical processing of aqueous atmospheric brown carbon. Atmos. Chem. Phys. 15 (2), 2957–2996.

Zhou, R., Wang, S., Shi, C., Wang, W., Zhao, H., Liu, R., Chen, L., Zhou, B., 2014. Study on the traffic air pollution inside and outside a road tunnel in Shanghai, China. PLoS One 9, e112195.

Zhou,Y.Q., Wang, Q.Y., Huang, R.J., Liu, S.X., Tie, X.X., Su, X.L., Niu, X.Y., Zhao, Z.Z., Ni, H.Y., Wang, M., Zhang, Y.G., Cao, J.J., 2017. Optical properties of aerosols and implications for radiative effects in Beijing during the Asia-Pacific Economic cooperation summit 2014. J. Geophys. Res. Atmos. 2017, 122(18).

Zhong, M., Jang, M., 2014. Dynamic light absorption of biomass-burning organic carbon photo chemically aged under natural sunlight. Atmos. Chem. Phys. 14, 1517-1525.

611
612
613
614
615
616
617
618
619
620
621
622
623
624
625

626 Figure Captions

627 Figure1 Location of the sampling site.

628 Figure 2 Diurnal variations of mean $b_{abs365,methanol}$, $b_{abs,\ BC\text{-}880nm}$, $MAC_{365,methanol}$, OC, Ox, and SOC

629 for $PM_{2.5}$ between haze and non haze days during (a) winter and (b) summer

630 Figure 3 the source contribution to $b_{abs365,methanol}$ using multivariate linear regression model

631 during (a) winter and (b) summer

632
633
634
635
636
637
638
639

640

641

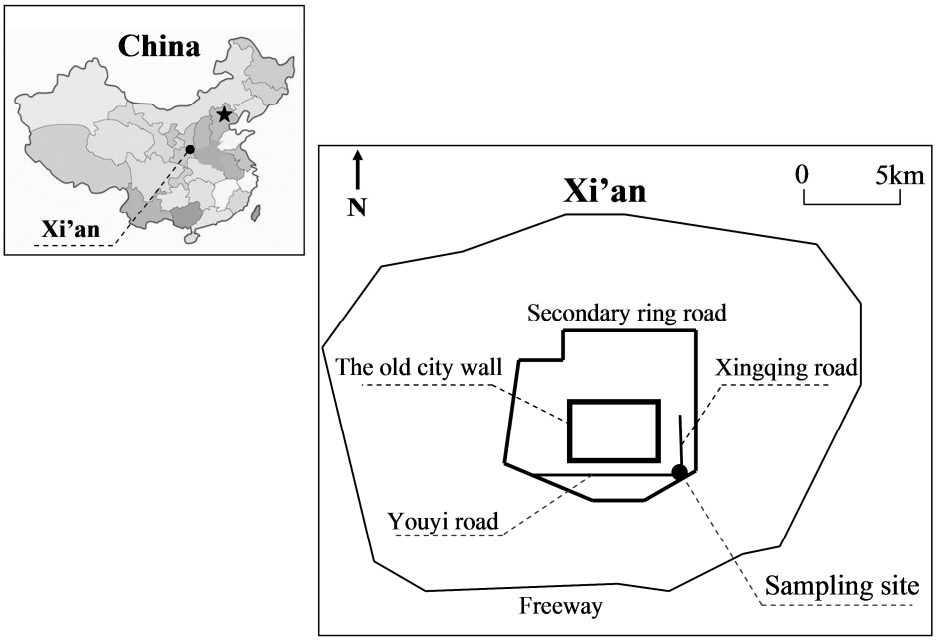

642

643

644 Figure1 Location of the sampling site.

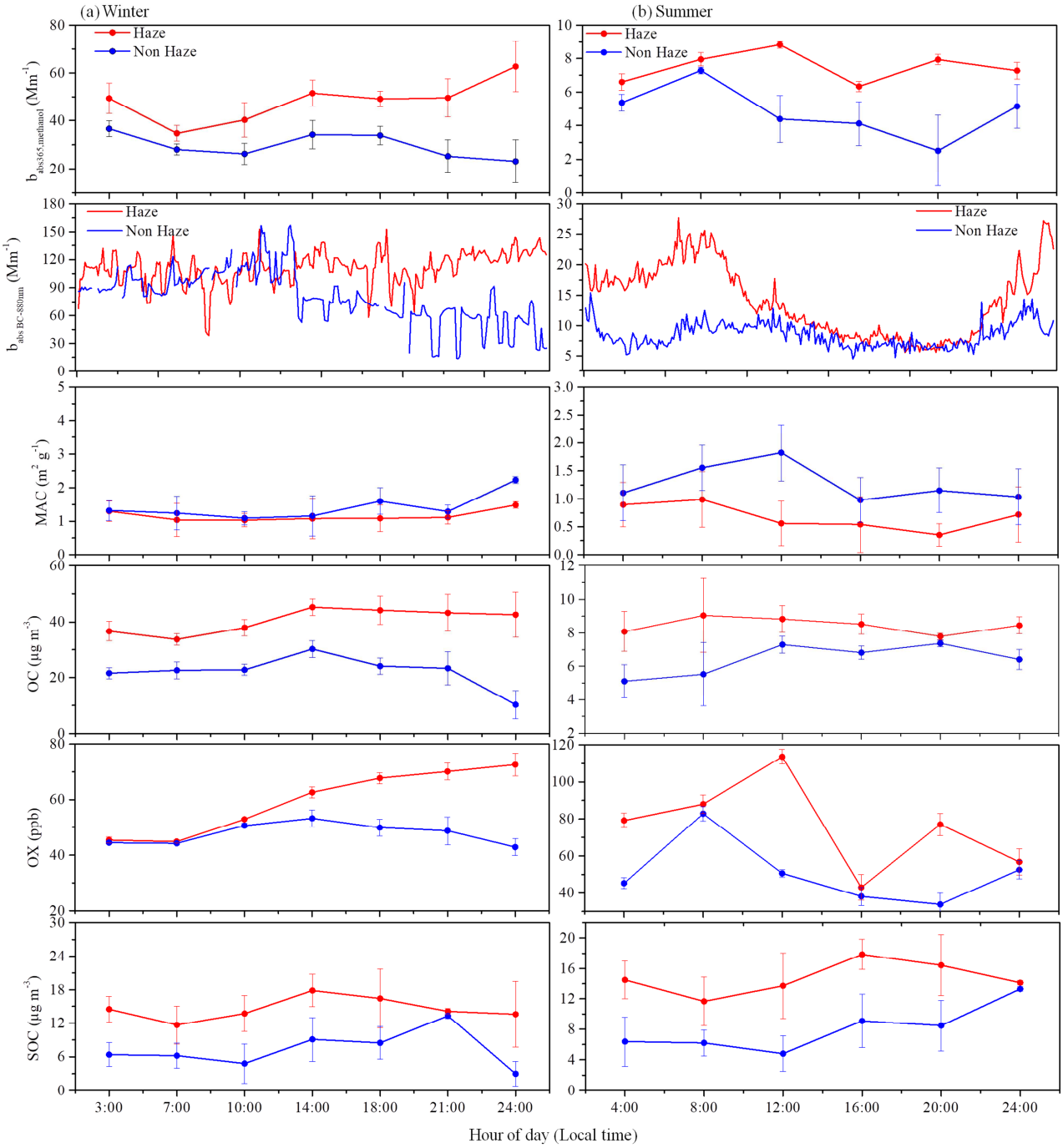

Figure 2 Diurnal variations of mean $b_{abs365,methanol}$, $b_{abs,\ BC-880nm}$, $MAC_{365,methanol}$, OC, Ox, and SOC for $PM_{2.5}$ between haze and non haze days during (a) winter and (b) summer

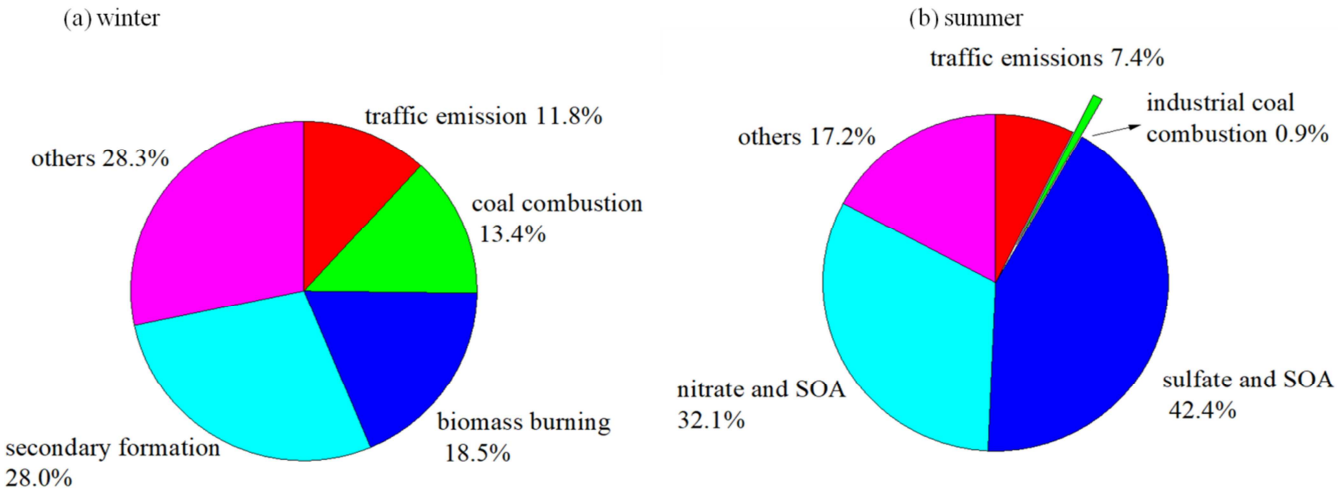

Figure 3 The source contribution to $b_{abs365,methanol}$ using multivariate linear regression model during (a) winter and (b) summer

Table 1 The average concentrations of major components and light absorption in $PM_{2.5}$ during the sampling period

Sampling period			$PM_{2.5}$	OC	SOC	EC	OC/EC	$b_{abs365,methanol}$	$b_{absBC-880nm}$	$MAC_{365,methanol}$	AAE
			$\mu g\ m^{-3}$					Mm^{-1}		$m^2\ g^{-1}$	330-400nm
winter	Total	mean	179.4	34.4	11.8	7.6	4.4	42.0	101.9	1.2	6.2
		SD	70.4	13.3	5.5	2.7	0.4	18.1	27.9	0.2	0.5
	Haze	mean	210.3	40.5	14.4	8.7	4.6	48.2	111.8	1.2	6.4
		SD	66.3	12.0	4.7	2.5	0.2	19.6	25.6	0.1	1.0
	Non-haze	mean	117.7	22.1	6.4	5.2	4.1	29.6	82.0	1.3	6.1
		SD	11.6	0.5	1.4	0.7	0.5	5.2	27.2	0.2	0.3
summer	Total	mean	69.7	7.7	4.0	5.6	1.6	5.9	11.8	0.9	6.5
		SD	18.8	1.8	1.8	1.5	0.6	2.8	3.6	0.6	2.6
	Haze	mean	74.8	8.0	4.4	5.6	1.6	6.8	11.9	1.0	6.5
		SD	17.0	2.0	2.3	1.8	0.6	2.9	4.7	0.7	2.3
	Non-haze	mean	65.3	7.4	3.7	5.6	1.5	4.9	11.6	0.7	6.5
		SD	20.5	1.6	1.4	1.1	0.6	2.6	2.3	0.4	3.1

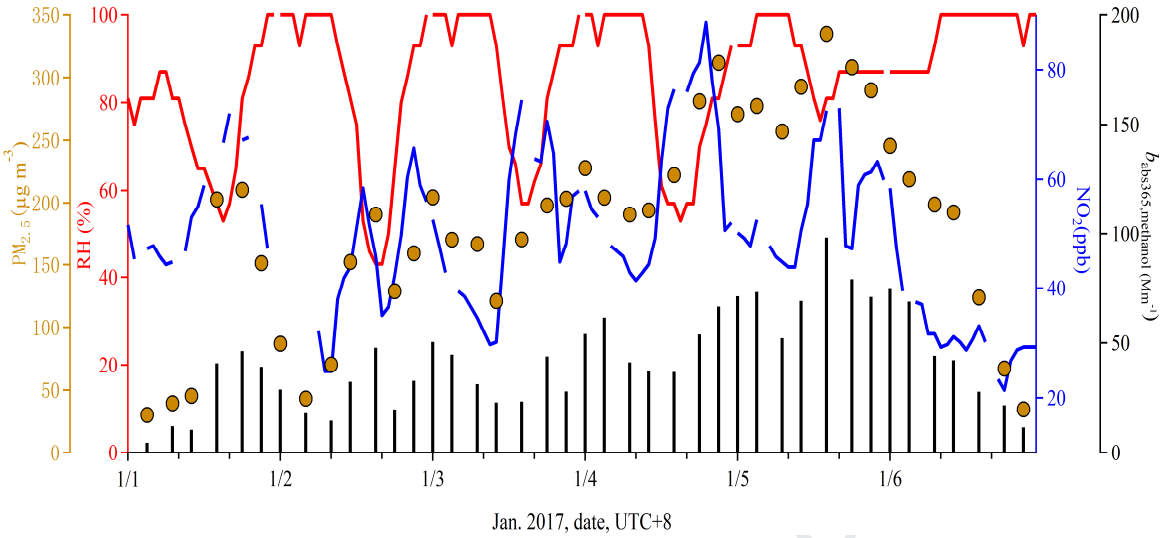

Figure 1S Daily variations of $PM_{2.5}$, RH, NO_2, and $b_{abs365,\ methanol}$ during the winter sampling period.

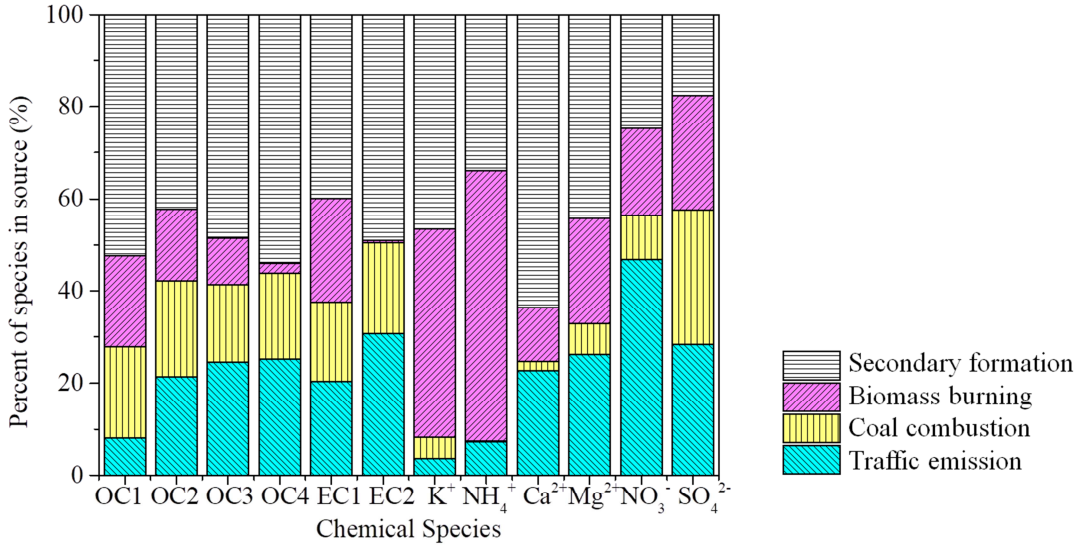

Figure S2 Source profiles for the four sources during winter identified by the positive matrix factorization (PMF) mode.

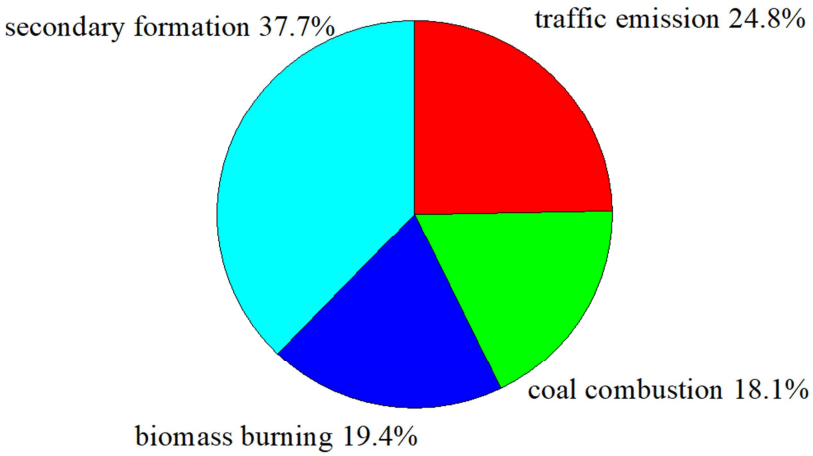

Figure S3 Average source contribution to aerosol mass concentration during winter that is estimated by PMF source factor (see Fig.S1)

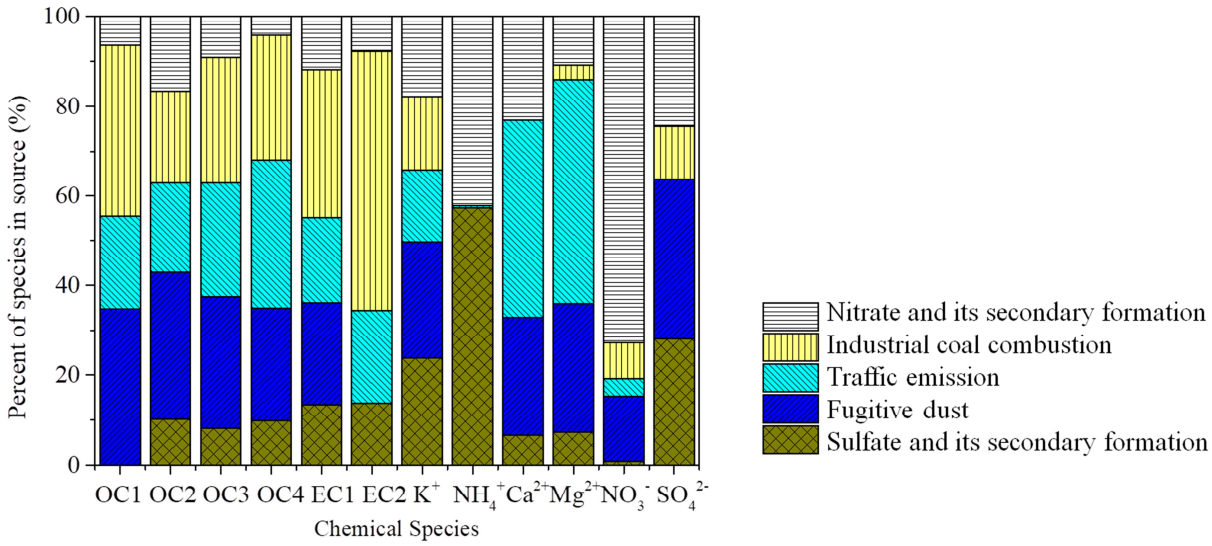

Figure S4 Source profiles for the five sources during summer identified by the positive matrix factorization (PMF) mode.

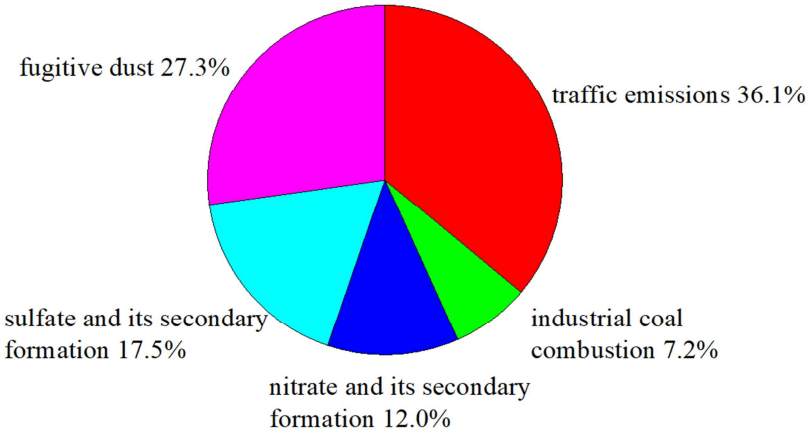

Figure S5 Average source contribution to aerosol mass concentration during summer that is estimated by PMF source factor (see Fig.S2)

Table S1 Regression diagnosis for each individual species and total mass $PM_{2.5}$ obtained by the PMF model (R^2= coefficient of determination).

Species	Intercept		Slope		R^2	
	winter	summer	winter	summer	winter	summer
$PM_{2.5}$ mass	22.36	26.33	0.89	0.64	0.96	0.71
OC1	0.62	0.59	0.58	0.25	0.63	0.87
OC2	0.43	0.22	0.93	0.87	0.95	0.75
OC3	3.48	0.15	0.6	0.92	0.77	0.86
OC4	3.89	0.31	0.25	0.88	0.79	0.82
EC1	5.98	1.29	0.73	0.63	0.87	0.7
EC2	0.03	0.07	0.91	0.88	0.77	0.96
K^+	0.2	0.41	0.91	0.51	0.91	0.81
NH_4^+	0.01	0.05	0.33	0.45	0.87	0.91
Mg^{2+}	0.11	0.11	0.75	0.75	0.74	0.74
Ca^{2+}	0.72	0.16	0.35	0.97	0.85	0.99
NO_3^-	0.34	0.03	0.67	0.54	0.88	0.92
SO_4^{2-}	0.56	0.8	0.77	0.65	0.93	0.86

Highlights

High time-resolved BrC observation during winter and summer was conducted.

Atmospheric aging can either enhance or reduce light absorption by BrC.

Primary emission and secondary formation were important contributors to BrC during winter and summer, respectively.